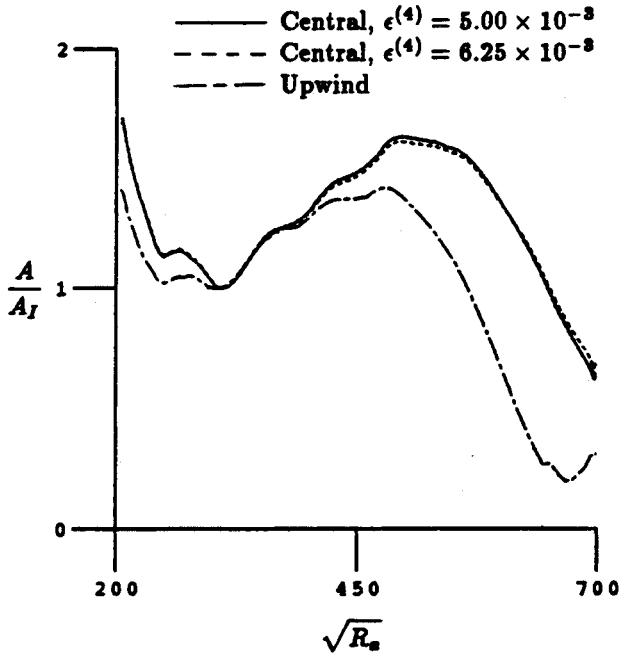

Fig. 4 Maximum streamwise momentum disturbance fluctuation vs Reynolds number at $M = 1.6$ and $\alpha = 0.11/\delta^*$ for upwind and central differencing on a 572 × 38 grid.

predicted by the PSE. The PSE also predicted a lower amplification than the present methods.

In conclusion, the requirements of two finite volume schemes as applied to the problem of fluid transition have been investigated. Calculations have been performed in both the subsonic and supersonic regimes. These schemes have been shown to be capable of predicting regions of stable and unstable flow that agree reasonably well with linear theory for low-amplitude disturbances. However, the resolution required to obtain useful results is somewhat high due to the level of accuracy of the numerical methods. Thus, there is a need to employ more accurate methods.

Acknowledgments

This work is supported in part by NASA's Cooperative Agreement NCCI-22, the Hypersonic Aerodynamic Program Grant NAGW-1022 funded jointly by NASA, the Air Force Office of Scientific Research, and the Office of Naval Research, and the Mars Mission Research Center funded by NASA Grant NAGW-1331. Some of the computer time was provided by the North Carolina Supercomputing Center.

References

[1]Wray, A., and Hussaini, M. Y., "Numerical Experiments in Boundary-Layer Stability," *Proceedings of the Royal Society of London,* Vol. A392, 1984, pp. 373–389.

[2]Zang, T. A., and Hussaini, M. Y., "Numerical Simulation of Nonlinear Interactions in Channel and Boundary-Layer Transition," *Nonlinear Wave Interactions in Fluids,* edited by R. W. Miksad, T. R. Akylas, and T. Herbert, ASME-AMD, Vol. 87, 1987, pp. 131–145.

[3]Laurien, E., and Kleiser, L., "Numerical Simulation of Boundary-Layer Transition and Transition Control," *Journal of Fluid Mechanics,* Vol. 199, 1989, pp. 403–440.

[4]Fasel, H. F., Rist, U., and Konzelmann, U., "Numerical Investigation of the Three-Dimensional Development in Boundary-Layer Transition," *AIAA Journal,* Vol. 28, No. 1, 1990, pp. 29–37.

[5]Spalart, P. R., and Yang, K., "Numerical Study of Ribbon-Induced Transition in Blasius Flow," *Journal of Fluid Mechanics,* Vol. 178, 1987, pp. 345–365.

[6]Bayliss, A., Parikh, P., Maestrello, L., and Turkel, E., "A Fourth-Order Scheme for the Unsteady Compressible Navier-Stokes Equations," AIAA Paper 85-1694, July 1985.

[7]Lele, S. K., "Direct Numerical Simulation of Compressible Free Shear Flows," AIAA Paper 89-0374, Jan. 1989.

[8]Jameson, A., Schmidt, W., and Turkel, E., "Numerical Solutions of the Euler Equations by Finite Volume Methods Using Runge-Kutta Time-Stepping Schemes," AIAA Paper 81-1259, 1981.

[9]Roe, P. L., "Characteristic-Based Schemes for the Euler Equations," *Annual Review of Fluid Mechanics,* Vol. 18, 1986, pp. 337–365.

[10]Macaraeg, M. G., Streett, C. L., and Hussaini, M. Y., "A Spectral Collocation Solution to the Compressible Stability Eigenvalue Problem," NASA TP-2858, 1988.

[11]Streett, C. L., and Macaraeg, M. G., "Spectral Multi-Domain For Large-Scale Fluid Dynamic Simulations," *Applied Numerical Mathematics,* Vol. 6, 1989, pp. 123–139.

[12]Bertolotti, F. P., "Linear and Nonlinear Stability of Boundary Layers with Streamwise Varying Properties," Ph.D. Dissertation, Ohio State Univ., Columbus, OH, 1990.

Freestream Capturing for Moving Coordinates in Three Dimensions

Shigeru Obayashi*
NASA Ames Research Center,
Moffett Field, California 94035

Introduction

BODY-CONFORMING coordinate transformations of a fluid conservation law are generally used in computational fluid dynamics. The associated metrics must satisfy certain geometric identities to maintain the global conservation for numerical solutions.[1] These metrics are called freestream capturing (or preserving) metrics. Numerical techniques are known to capture the freestream on stationary grids.[2-4] However, the extension of such a formulation for moving grids is not straightforward. The error introduced in forming the time metrics has been overlooked because it is negligible in most cases, but it can be significant in certain applications such as helicopter rotor flows.[5] Rigorous formulations based on the types of grid motions were discussed in Ref. 1, and demonstrated, for example, in Ref. 6. The present study describes detailed formulas that can be used in both finite volume (FV) and finite difference (FD) methods for constructing freestream capturing metrics in space and time.

Finite Volume Formulation

Geometric Identities and Freestream Capturing

The integral form of a conservation law for a given cell can be written as

$$\int_{V(t_2)} Q\,\mathrm{d}V - \int_{V(t_1)} Q\,\mathrm{d}V + \int_{t_1}^{t_2} \oint_{S(t)} \boldsymbol{n}\cdot\boldsymbol{F}\,\mathrm{d}S\,\mathrm{d}t = 0 \qquad (1)$$

where $V(t)$ is the cell volume and $\boldsymbol{n}\,\mathrm{d}S(t)$ is a vector element of surface area with outwardly normal $\boldsymbol{n}$. Considering the Euler equations, Q is a vector of conserved variables, viz., density, momentum, and energy, and $\boldsymbol{F}$ is the flux tensor of Q. The flux $\boldsymbol{F}$ can be decomposed into the flux in the stationary frame $\boldsymbol{F}_{\mathrm{st}}$ and the contribution due to surface element velocity $\boldsymbol{v}$ as

$$\boldsymbol{F} = \boldsymbol{F}_{\mathrm{st}} - \boldsymbol{v}Q \qquad (2)$$

Received Nov. 27, 1990; revision received June 10, 1991; accepted for publication June 24, 1991.

*Senior Research Scientist, MCAT Institute, San Jose, CA 95127.

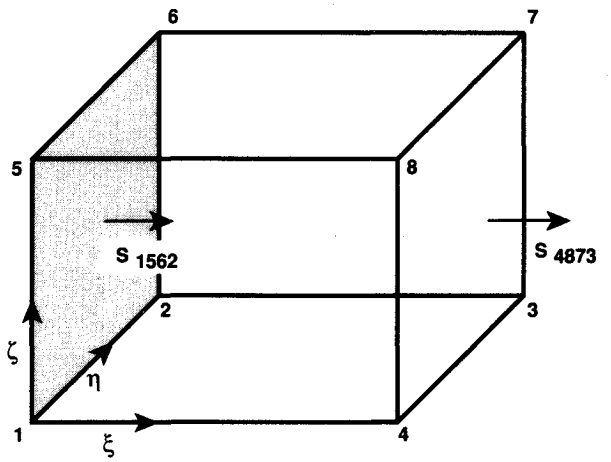

Fig. 1 Geometry of a hexahedral cell.

For the freestream condition Q_∞ and $F_{st\infty}$ the geometric identities can be derived from Eq. (1) as follows:

$$Q_\infty[V(t_2) - V(t_1)] = -F_{st\infty} \cdot \int_{t_1}^{t_2} \oint_S n \, dS \, dt + Q_\infty \int_{t_1}^{t_2} \oint_S n \cdot v \, dS \, dt \tag{3}$$

On a stationary grid, the first geometric identity can be obtained as

$$\oint_S n \, dS = 0 \tag{4}$$

This gives a mathematical expression for a closed cell, which is a requirement for any grid system. The corresponding time integration in Eq. (3) will be satisfied for moving grids by applying Eq. (4) at each time level. From the rest of Eq. (3), the second geometric identity can be obtained as

$$V(t_2) - V(t_1) = \int_{t_1}^{t_2} \oint_{S(t)} n \cdot v \, dS \, dt \tag{5}$$

This equation is essential for moving grids because it represents the conservation of volume for a moving cell. To guarantee the global conservation for numerical solutions, these geometric identities must be satisfied numerically.

Figure 1 shows a regular hexahedral cell. We assume that all edges are straight lines. Let r be the position vector of a point in space. The formulas for the surface vector S (note that S is taken in the positive coordinate direction here) and the volume V can be defined as

$$S_{1562} = \tfrac{1}{2}(r_6 - r_1) \times (r_5 - r_2) \tag{6}$$

$$S_{1562} = (r_{56} - r_{12}) \times (r_{15} - r_{26}) \tag{7}$$

$$V_{12345678} = \tfrac{1}{3}(S_{1485} + S_{1234} + S_{1562}) \cdot (r_7 - r_1) \tag{8}$$

where $r_{56} = \tfrac{1}{2}(r_5 + r_6)$, and so on (see Ref. 1, for example). Note that Eqs. (6) and (7) result in the same expression. In fact, the surface vector is defined uniquely as long as the edges are straight lines. Also note that there are other consistent ways to compute the cell volume. However, Eq. (8) is the simplest form.

Let $S_{1562} = S_{1562}n$. With either Eq. (6) or (7), Eq. (4) is satisfied numerically as

$$\sum_{\text{cell}} Sn = 0 \tag{9}$$

To satisfy Eq. (5) numerically, it is essential to compute the right-hand side correctly. It can be rewritten as

$$\int_{t_1}^{t_2} \oint_S n \cdot v \, dS \, dt = \int_{t_1}^{t_2} \left(\sum_{\text{cell}} Sn \cdot v \right) dt = \sum_{\text{cell}} \left(\int_{t_1}^{t_2} Sn \cdot v \, dt \right) \tag{10}$$

Let V_S be a volume swept by a surface S between the time interval $[t_1,t_2]$:

$$V_S = \int_{t_1}^{t_2} Sn \cdot v \, dt \tag{11}$$

Let $S(t_1) = S_{1562}$ and $S(t_2) = S_{1'5'6'2'}$. The volume V_S can be computed similar to Eq. (8) as

$$V_{S_{1265}} = V_{122'1'566'5'} = \tfrac{1}{3}(S_{11'5'5} + S_{122'1'} + S_{1562}) \cdot (r_{6'} - r_1) \tag{12}$$

where $S_{11'5'5}$ and $S_{122'1'}$ are the surface vectors in space and time domain. Then, Eq. (5) is satisfied numerically as

$$V(t_2) - V(t_1) = \sum_{\text{cell}} V_S \tag{13}$$

This formula requires the position of the grid at t_2, not the grid velocity v itself as per Eq. (11). The position of the grid at the next time level must be given explicitly before computing the fluid motion. For aeroelastic simulations, for example, the structural equation of motion has to be coupled with the fluid equations only at explicit time levels. A fully coupled implicit formulation requires an iterative approach between the fluid and structural equations.

Geometric Identities for Time-Differential Form

The time-differential form of Eq. (1) is often used as a basis of the conservation law. Starting with the time-differential form, one can obtain similar geometric identities as in the previous section. However, this approach introduces an additional geometric identity.

The first geometric identity derived from the time-differential form is identical to Eq. (4). Then, the rest of the equation can be written as

$$\frac{\partial V}{\partial t} = \oint_S n \cdot v \, dS \tag{14}$$

To proceed with the surface integration on the right-hand side, let us break down the surface element velocity v into its components. Let r and $r_0(t)$ be the position vectors of a point in space and the origin of the noninertial frame, respectively. Also let $v_0(t)$ and $\Omega(t)$ be the velocity and angular velocity of the noninertial frame relative to the inertial frame, respectively. These velocities represent the rigid motion of the grid. In general,

$$v = v_0(t) + \Omega(t) \times [r - r_0(t)] + v_c \tag{15}$$

where $v_c(t)$ is the surface element velocity relative to the noninertial frame, which leads to change of a cell in time. From Eqs. (14) and (15), one obtains

$$\frac{\partial V}{\partial t} = (v_0 - \Omega \times r_0) \cdot \left(\oint_S n \, dS \right) + \Omega \cdot \left(\oint_S r \times n \, dS \right) + \left(\oint_S n \cdot v_c \, dS \right) \tag{16}$$

The first integral on the right-hand side is zero due to the first geometric identity, Eq. (4). The second integral represents the rigid rotation of grid and does not contribute to the change of the cell volume. The remaining terms give the second geometric identity similar to Eq. (5).

The third geometric identity can be obtained from the second integral in Eq. (16) as

$$\oint_S \boldsymbol{r} \times \boldsymbol{n}\, dS = 0 \tag{17}$$

The discretized form of the third geometric identity can be expressed as

$$\sum_{\text{cell}} S\boldsymbol{r} \times \boldsymbol{n} = 0 \tag{18}$$

This is the additional requirement, which is concealed unless the grid movement is broken down properly. It must be satisfied whenever the grid rotates. Reference 1 introduces the area moment

$$\boldsymbol{M} = \int_S \boldsymbol{r} \times \boldsymbol{n}\, dS$$

to satisfy the discretized geometric identity, Eq. (18), on the hexahedron:

$$\boldsymbol{M}_{1562} = \boldsymbol{r}_{165} \times \boldsymbol{S}_{165} + \boldsymbol{r}_{126} \times \boldsymbol{S}_{126} \tag{19}$$

where $\boldsymbol{r}_{165} = \frac{1}{3}(\boldsymbol{r}_1 + \boldsymbol{r}_6 + \boldsymbol{r}_5)$, $\boldsymbol{S}_{165} = \frac{1}{2}(\boldsymbol{r}_6 - \boldsymbol{r}_1) \times (\boldsymbol{r}_5 - \boldsymbol{r}_1)$, and so on. Note that $\boldsymbol{M}_{1562} \neq \boldsymbol{r}_{1562} \times \boldsymbol{S}_{1562}$. The expression $\boldsymbol{r}_{1562} \times \boldsymbol{S}_{1562}$ is not well defined for computing area moment because it results in a nonzero sum over a cell. In contrast, Eq. (19) is well defined so that the sum over a cell is zero. The nonzero error introduced by the use of the inconsistent area moment has a unique feature. A simple analysis[7] shows that the error disappears on a hexahedron with parallelogram surfaces, for example, on the Cartesian grid. For a hexahedron with arbitrary quadrilateral surfaces, the error remains constant relative to the cell volume. This error may be ignored only if the effect of the Coriolis force is negligible. For example, the error is small for a flow over a wing oscillating at small amplitude. Note that the use of the surface area vector for evaluating the surface moment vector becomes consistent on a triangular surface. The use of the tetrahedral cell allows the most compact and consistent metric formulation, although it results in unstructured-grid formulations.

Finite Difference Formulation

The differential form of Eq. (1) has been used widely in FD formulations. With a generalized coordinate transformation, $\boldsymbol{r} = \boldsymbol{r}(\xi,\eta,\zeta,\tau)$ and $t = \tau$, the FD metric terms can be expressed as

$$\frac{\nabla\xi}{J} = \frac{1}{J}(\xi_x, \xi_y, \xi_z)^T = \boldsymbol{r}_\eta \times \boldsymbol{r}_\zeta = \boldsymbol{S}^\xi \tag{20}$$

and

$$\frac{\xi_t}{J} = -\boldsymbol{S}^\xi \cdot \boldsymbol{r}_\tau \tag{21}$$

where $\boldsymbol{r}_\tau = \boldsymbol{v}$ and the transformation Jacobian $J = 1/V$. Analogous definitions can be derived for the other directions. The cell volume as defined by Eq. (8) is different from the inverse of the transformation Jacobian in a discretized form. Nevertheless, the cell volume can be applied to the FD method with a scaling factor of one-eighth. The differential forms of the geometric identities are

$$(\boldsymbol{S}^\xi)_\xi + (\boldsymbol{S}^\eta)_\eta + (\boldsymbol{S}^\zeta)_\zeta = 0 \tag{22}$$

$$V_\tau = (\boldsymbol{S}^\xi \cdot \boldsymbol{r}_\tau)_\xi + (\boldsymbol{S}^\eta \cdot \boldsymbol{r}_\tau)_\eta + (\boldsymbol{S}^\zeta \cdot \boldsymbol{r}_\tau)_\zeta \tag{23}$$

Equation (23) is the differential statement of the geometric conservation law (GCL).[8]

The discretized form of Eq. (22) can be satisfied by the consistently differenced metrics,[3] which are based on an averaging procedure to numerically satisfy the differential chain rule. However, it is not straightforward to satisfy the discretized form of the GCL. The discretized form of the GCL can be written as

$$\Delta V = \Delta\tau[\delta_\xi(\boldsymbol{S}^\xi \cdot \boldsymbol{r}_\tau) + \delta_\eta(\boldsymbol{S}^\eta \cdot \boldsymbol{r}_\tau) + \delta_\zeta(\boldsymbol{S}^\zeta \cdot \boldsymbol{r}_\tau)] \tag{24}$$

where δ indicates the central-difference operator in each coordinate direction. Analogous to the derivation of Eq. (18), if the grid is moved in a rigid rotation, $V_\tau = 0$ and $\boldsymbol{r}_\tau = \Omega \times \boldsymbol{r}$. Then the left-hand side of Eq. (24) equals zero. However, the right-hand side becomes $\delta_\xi(\boldsymbol{r} \times \boldsymbol{S}^\xi) + \delta_\eta(\boldsymbol{r} \times \boldsymbol{S}^\eta) + \delta_\zeta(\boldsymbol{r} \times \boldsymbol{S}^\zeta) \neq 0$. Thus, the freestream will not be captured by solving Eq. (24) with the FD method. The GCL implies only a necessary condition to capture the freestream, not a sufficient condition.

The analysis of the FD formulation can be simplified with the aid of the previous discussions for the FV formulations. Following Ref. 1, let the edges of the hexahedron in Fig. 1 be redefined as a double-sized cell in the FD grid with $\boldsymbol{r}_1 = \boldsymbol{r}_{i-1,j-1,k-1}$, $\boldsymbol{r}_2 = \boldsymbol{r}_{i-1,j+1,k-1}$, . . . , $\boldsymbol{r}_3 = \boldsymbol{r}_{i+1,j+1,k-1}$, $\boldsymbol{r}_8 = \boldsymbol{r}_{i+1,j-1,k+1}$. Also, let the time level advance from t_1 to t_2. A simple calculation[7] shows that Eq. (7) is equivalent to the consistently differenced metrics.[3] Thus, the surface vector evaluations, Eqs. (6) and (7), on the double-sized cell can be regarded as the evaluations of the freestream capturing space metrics for the FD method. The FD time-metric evaluation is also obtained from the FV method. Time integration of Eq. (24) from t_1 to t_2 easily results in Eq. (13). Thus, for example in the ξ direction, replacing $\boldsymbol{S}^\xi \cdot \boldsymbol{r}_\tau$ in the right-hand side of Eq. (21) with the time average, $V_{S\xi}/\Delta t$ of Eq. (11), the freestream capturing time metrics can be obtained as

$$\frac{\xi_t}{J} = -\frac{1}{\Delta t}\int_{t_1}^{t_2} \boldsymbol{S}^\xi \cdot \boldsymbol{r}_\tau\, dt = -\frac{V_{S\xi}}{\Delta t} \tag{25}$$

Note that ξ_t defined here is costly but contains all of the information about the movement of a cell surface, such as translation, rotation, and deformation. In contrast, Eq. (21) is a simple product of surface area and velocity of cell centroid and can represent only a translational motion.

The freestream subtraction technique will be useful for the rigid motion of the grid instead of the rigorous, costly evaluation of Eq. (25). Note that the subtraction is required only for the time-metric terms with the use of the freestream capturing metrics in space.[5]

Concluding Remarks

This Note discusses the freestream capturing and the geometric identities for a fluid conservation law. To guarantee global conservation in numerical solutions, certain geometric identities must be satisfied. Based on the full integral form of the conservation law, Eqs. (7), (8), and (13) will guarantee the freestream capturing. Based on the time-differential form, another condition [Eq. (18)] must also be satisfied. However, when the differential form is used, the global conservation is not trivial. Considering an FV cell on the FD grid, the freestream capturing metrics in space and time can be constructed from the FV formulations. Such an approach for evaluating the time metrics is costly but guarantees the global conservation for an arbitrary motion of the grid.

Acknowledgments

This work was supported by NASA Grant NCC 2-605. The author would like to thank M. Vinokur of Sterling Software for his valuable discussions.

References

[1]Vinokur, M., "An Analysis of Finite-Difference and Finite-Volume Formulations of Conservation Laws," *Journal of Computational Physics*, Vol. 81, No. 1, 1989, pp. 1-52.

[2]Pulliam, T. H., and Steger, J. L., "On Implicit Finite-Difference Simulations of Three-Dimensional Flow," AIAA Paper 78-10, Jan. 1978.

[3]Chaderjian, N. M., "Transonic Navier-Stokes Wing Solutions Using a Zonal Approach," NASA TM-88248, April 1986.
[4]Buning, P. G., Chiu, I. T., Obayashi, S., Rizk, Y. M., and Steger, J. L., "Numerical Simulation of the Integrated Space Shuttle Vehicle in Ascent," AIAA Paper 88-4359, Aug. 1988.
[5]Srinivasan, G. R., Baeder, J. D., Obayashi, S., and McCroskey, W. J., "Flowfield of a Lifting Hovering Rotor—A Navier-Stokes Simulation," 16th European Rotorcraft Forum, Paper I.3.5, Glasgow, Scotland, UK, Sept. 1990; also NASA TM-102862, Aug. 1990.
[6]Chen, C. L., and McCroskey, W. J., "Numerical Simulation of Helicopter Multi-Bladed Rotor Flow," AIAA Paper 88-0046, Jan. 1988.
[7]Obayashi, S., "Free-Stream Capturing in Fluid Conservation Law for Moving Coordinates in Three Dimensions," NASA CR-177572, Jan. 1991
[8]Thomas, P. D., and Lombard, C. K., "Geometric Conservation Law and Its Application to Flow Computations on Moving Grids," *AIAA Journal*, Vol. 17, No. 10, 1979, pp. 1030–1037.

Semi-Inverse Marching Characteristics Scheme for Supersonic Flows

Joseph Falcovitz* and Allen E. Fuhs†
Naval Postgraduate School, Monterey, California 93941

Nomenclature

$C^{\pm}$ = characteristic lines corresponding to $\theta \pm \mu$
$R^{\pm}$ = Riemann invariants along $C^{\pm}$, $(\nu \mp \theta)$
M = Mach number
x,y = Cartesian coordinates
Γ = $[(\gamma + 1)/(\gamma - 1)]^{1/2}$
γ = specific heats ratio
δ = symmetry index (zero planar flow, one axisymmetric flow)
θ = inclination of flow velocity vector relative to x axis
μ = Mach angle, $\sin \mu = M^{-1}$
ν = Prandtl-Meyer function $\nu(M) = \Gamma \arctan(\Gamma^{-1}\sqrt{M^2 - 1}) - \arctan(\sqrt{M^2 - 1})$

Introduction

THE purpose of this Note is to present a modification of the inverse marching characteristics scheme for compressible flows that is designed to yield an exact computation of centered rarefaction waves, such as the Prandtl-Meyer corner expansion flow (PMF). The key idea is to combine a semi-inverse marching scheme (grid points near corner are located on continuous characteristics emanating from the corner) with the designation of Riemann invariants as flow variables. The resulting semi-inverse marching algorithm (SIMA) scheme replicates a Prandtl-Meyer flow accurately, while yielding the solution on a relatively regular grid. In this Note, the SIMA scheme is presented following a brief discussion of the background and then its accuracy is demonstrated by considering a planar plume flow.

The inverse marching method of characteristics[1] is a standard scheme for the computation of compressible isentropic flow in two dimensions. Two instances of flow are possible: either the time-dependent compressible flow in x,t or the steady supersonic flow in x,y. We shall restrict our discussion to the latter. (The time-dependent case can be treated in a very similar fashion.) To fix ideas, we assume a supersonic exit flow, where the characteristic lines $C^{\pm}$ (corresponding to $\theta \pm \mu$) propagate in the positive y direction as depicted in Fig. 1. (However, if this condition does not hold, lines of y = const may be replaced by a set of curves such that $C^{\pm}$ characteristics propagate forward from every point on each curve.) The advantage of the inverse marching algorithm (IMA) scheme is that it yields a solution on a relatively regular grid of points, whereas the direct method of characteristics[1] renders the flowfield at an irregular grid formed by the intersection of C^- and C^+ characteristic lines and their reflections from boundaries.

The IMA scheme consists in seeking the flow at new grid points (x_{ij},y_j) located on a new row $y = y_j$, where the new row is obtained from an old row by a forward marching step: $y_j = y_{j-1} + \Delta y_{j-1}$. The number and distribution of grid points on each new row is independent of their distribution on the old row. The recommended flow variables are velocity components [Ref. 1, Secs. 12-5(b) and 13-5(a)].

To determine the flow at grid points of a new row, C^- and C^+ characteristics are inversely extended from each new point until they intersect the old row $y = y_{j-1}$ at corresponding C^- or C^+ trace points (Fig. 2). The flow at each new grid point is then obtained from the C^- and C^+ compatibility relations that are approximated by a pair of centered implicit finite difference equations.[1] It has been found that by applying the IMA scheme to a PMF having a uniform supersonic flow on its upstream side, the computed results deviated appreciably from the known analytic (self-similar) solution. The reasons for errors in computing a corner flow by the IMA scheme are well understood. Two factors contribute to these errors:

1) There is an error in locating old trace points by inversely extending $C^{\pm}$ characteristic lines from new grid points.

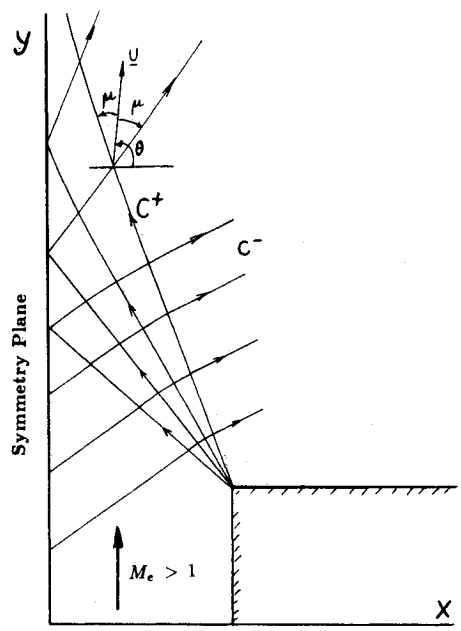

Fig. 1 Reflection of Prandtl-Meyer fan from symmetry plane (schematic).

Received Jan. 8, 1991; revision received June 30, 1991; accepted for publication July 19, 1991. This paper is declared a work of the U.S. Government and is not subject to copyright protection in the United States.

*Senior Research Professor, Space Systems Academic Group; currently, Faculty of Aerospace Engineering, Technion, Haifa, Israel.
†Chairman, Space Systems Academic Group; currently, Distinguished Professor (Emeritus). Fellow AIAA.